# Laser spectroscopy of molecular LiHe: The $3d\ ^2\Delta \leftarrow 2p\ ^2\Pi$ transition

C. J. Lee, M. D. Havey, and R. P. Meyer
*Physics Department, Old Dominion University, Norfolk, Virginia 23529*
(Received 13 August 1990)

The rotationally resolved absorption spectrum of the $3d\ ^2\Delta \leftarrow 2p\ ^2\Pi$ transition in molecular LiHe has been measured. For each of three isotropic variants $^6Li^3He$, $^6Li^4He$, and $^7Li^4He$, six vibrational transitions have been observed from the lower $2p\ ^2\Pi(v''=0,1)$ electronic state to the upper $3d\ ^2\Delta(v'=0,1,2,3)$ electronic state. Analysis of the observed spectra has yielded values for the well depth and equilibrium separation of 1020(20) $cm^{-1}$ at $3.37(3)a_0$ for the $2p\ ^2\Pi$ state and 610(20) at $3.52(2)a_0$ for the $3d\ ^2\Delta$ state. Details of our analysis and our experimental technique are presented.

## I. INTRODUCTION

The interaction of alkali and rare-gas atoms has for many years been the object of considerable experimental and theoretical study. A principal stimulus for this research has been a desire to obtain a basic understanding of a wide range of collision processes, including electronic energy transfer, fine-structure transitions, depolarization and coherence transfer, and line broadening and shifts. Measurements of these various processes have brought out the need for accurate potentials, in the range of chemical forces, for excited alkali–rare-gas molecular states. The interaction potentials are essential to an understanding of the collision processes in general, and specifically to theoretical calculations of cross sections for them. Processes depending strongly on angular momentum decoupling and recoupling during a collision[1,2] (coherence transfer and fine-structure transitions, for example) depend sensitively on the shapes and relative sizes of the pertinent molecular terms. Even extremely weak processes such as spin-relaxation and spin-exchange in alkali *s*-state–rare-gas collisions depend,[3] primarily through molecular formation and breakup rates, on the range and depth of the molecular potentials. The basic long-range interactions between alkali and rare-gas atoms are also of interest in their own right, and considerable effort has gone into devising methods of computing them.[4–18]

A number of experimental techniques have been applied to learning the alkali–rare-gas interatomic potentials. Of these, far-wing line broadening,[19–25] atomic beam scattering,[26–32] and rotationally resolved laser spectroscopy[33–40] have yielded the most consistent results. These studies, along with the most reliable theoretical ones, have led to recognition of certain regularities in the binding energies and equilibrium separations in the lower electronic states of these molecules.[4]

For example, if we consider the lowest $^2\Pi$ state of a particular alkali–rare-gas molecule, the binding energy is known to increase regularly as one changes the rare gas from Ne through Xe, reflecting the increasing polarizability of the rare gas. In this same example, the approximate constancy of the rare-gas size for this state leads to a $^2\Pi$ equilibrium position that is nearly independent of the rare gas. Furthermore, as one varies the alkali for each rare gas, the $^2\Pi$ state binding increases from Cs to Li, and the equilibrium separation decreases. This behavior may be considered to at least partly result from the decreasing average size of the alkali atom or, equivalently, a decrease in the range of the repulsive part of the alkali-atom–rare-gas interaction.

Recent experimental[23,24,38] and theoretical[4,9,15,41] results have indicated that the alkali-He diatomic pairs do not fit into this general scheme. In these cases, a penetration of the He $1s^2$ core by the diffuse alkali atom $\pi$ orbital results in a smaller equilibrium separation and a considerably deeper $A\ ^2\Pi$ state well than would be expected from the trends just discussed.

We have an ongoing experimental program of laser spectroscopy of the alkali–rare-gas diatomic molecules. A main goal of the experiments is to obtain rotationally resolved spectra of various excited-state transitions in these molecules and to invert the spectra to obtain associated interaction potentials. We have previously reported[38] preliminary results on the $^7Li^4He$ $3d\ ^2\Delta \leftarrow 2p\ ^2\Pi$ transition. Subsequent improvements in spectral resolution and sensitivity have led to considerably more detailed spectroscopic data on this and several other transitions out of the $2p\ ^2\Pi$ electronic state. We present in this paper the details of our experimental method and our measurments and results on the $3d\ ^2\Delta \leftarrow 2p\ ^2\Pi$ transition in $^6Li^3He$, $^6Li^4He$, and $^7Li^4He$. A later paper will report our results on the $3p\ ^2\Sigma^+ \leftarrow 2p\ ^2\Pi$, $3d\ ^2\Pi \leftarrow 2p\ ^2\Pi$, and $3p\ ^2\Pi \leftarrow 2p\ ^2\Pi$ transitions for the same three LiHe isotopic variants.

We have further completed spectroscopic studies of several electronic transitions in LiNe; these include transitions to the $3s\ ^2\Sigma^+$, $3d\ ^2\Delta$, $3d\ ^2\Pi$, $3d\ ^2\Sigma^+$, and $3p\ ^2\Sigma^+$ states from the $2p\ ^2\Pi$ state. The results will be presented later in a series of papers following this one.

The remainder of this paper is organized as follows. First we give details of our experimental scheme and methodology. This is followed by the results of our spectroscopic measurements and analysis of the observed spectra. Comparison of our results with recent theoretical calculations and other experiments on LiHe is then made.

 

## II. EXPERIMENT

### A. General experimental method

The lowest $X\,^2\Sigma^+$ electronic state of the alkali–rare-gas (AR) molecules is very weakly bound, showing a typical binding energy of less than $\sim 100$ cm$^{-1}$ and a well minimum around $10a_0$. This has limited rotationally resolved spectroscopic studies of these molecules to a few cases (Na-Ne, Na-Ar, Na-Kr), where they have been produced in supersonic expansions.[33–40] The excited states, however, can show substantial binding ($\sim 1000$ cm$^{-1}$); our experimental technique for generating rotationally resolved LiHe spectra is based on the significant binding in the $2p\,^2\Pi$ first excited molecular state.[4,15]

The experimental scheme can be generally understood with reference to Fig. 1, which illustrates qualitative interatomic potentials for LiHe. In this scheme, laser 1 resonantly excites Li atoms to the atomic $2p$ state. Subsequent three-body collisions, mainly with two He atoms, produce bound LiHe molecules in the $2p\,^2\Pi$ electronic state. A second laser scans over the manifold of electronic transitions[42] shown in Fig. 1 with sufficient resolution to excite individual rotational-vibrational transitions. The excited molecules thus produced then dissociate by predissociation or by collisions with He atoms, producing atomic Li population in the $3d$ and $3p$ states. The $3d$ and $3p$ populations are nearly thermalized within the excited state lifetime for a He pressure of 50 Torr.[43,44] Near ultraviolet $3p \rightarrow 2s$ atomic Li emission at 323.4 nm is monitored as the signature of a molecular LiHe absorption.

### B. Experimental details

A schematic diagram of our experimental apparatus is presented in Fig. 2. Mixtures of ground-state Li and He atoms were produced in an experimental cell consisting of a 250-cm$^3$ Pyrex flask mounted with a 10-mm-o.d. quartz sidearm. An iron boat containing Li metal and located within the sidearm was resistively heated to about 1000 K, producing an estimated Li density of $10^{12}$ cm$^{-3}$ in the central region of the cell. Cells containing either $^6$Li or $^7$Li isotopes were used. The cell also contained 10–150 Torr of research grade $^3$He or $^4$He; the cell was filled with He gas at 295 K. The gas pressure was measured with a capacitance manometer having an accuracy of about 0.1 Torr. The cell was permanently attached to an oil-free vacuum-gas handling system; the base pressure was about $10^{-8}$ Torr. For cells of this type, previous measurements[24] have shown that the central region of the cell is at a temperature approximately given by the average wall temperature. In the experiments described here, this was about 350 K, consistent with the rotational temperature[42] of the observed LiHe spectra. A difficulty with the cell was the eventual coating of the relatively cool cell walls with alkali metal. In our case, the coating consisted of Li and Na, which was present in significant amounts in our Li samples. For longer experimental runs ($>5$ h), it was necessary to cool the Li reservoir and to drive the metal from the cell walls with a flame; the He gas was removed from the cell during this operation. Addition of extended entrance and exit ports for the laser

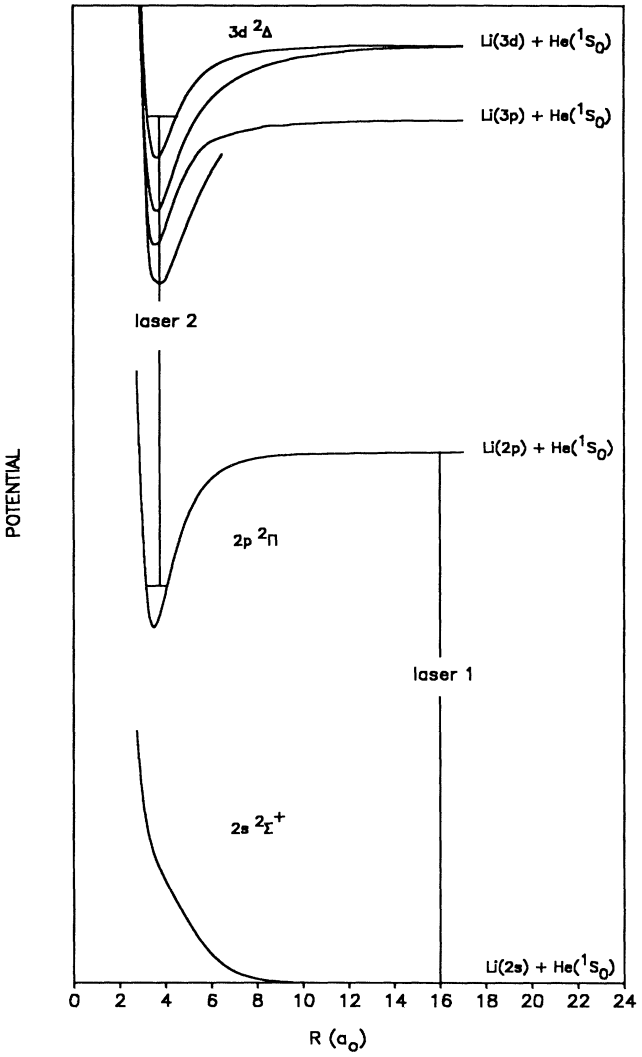


FIG. 1. Qualitative interaction potentials for selected LiHe molecular states. The vertical axis is not to scale.

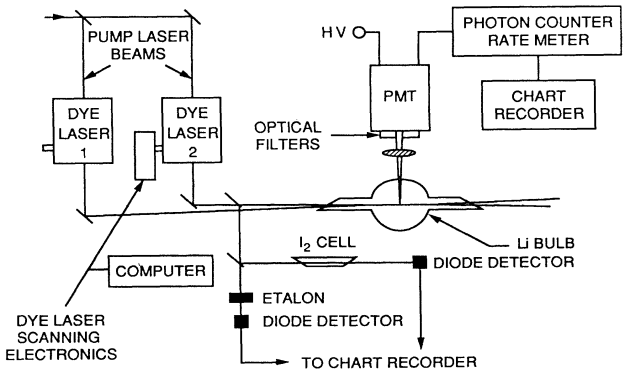


FIG. 2. A schematic diagram of the experimental apparatus.

beams and a fluorescence viewing port practically eliminated this difficulty.

Li atoms were excited to the $2p$ state by an $Ar^+$ pumped cw dye laser (laser 1) tuned to the Li $2s$-$2p$ resonance transition at 671.0 nm. The laser was tuned and passively stabilized with a birefringent-filter–solid-etalon combination, which produced a linewidth of about 0.2 $cm^{-1}$; the etalon was an uncoated, 0.10-cm-thick quartz plate mounted on an electronically scanned galvanometer, which was used to fine tune the laser frequency. The laser linewidth quite well matched the overall width ($\sim$0.15 $cm^{-1}$) of the Doppler- and collision-broadened Li resonance transitions. The atomic Li $2p$ fine-structure splitting is about 0.34 $cm^{-1}$. Laser 1 produced a linearly polarized output of around 200 mW.

Laser 2 was an $Ar^+$-laser pumped cw ring dye laser that produced a linearly polarized output of approximately 300 mW in an average linewidth of about 0.05 $cm^{-1}$. Smooth frequency scanning was accomplished by a synchronously scanned three plate birefringement-filter–solid-etalon combination. A computer-controlled stepper motor rotated the birefringent filter. The stepping rate necessary to achieve a linear frequency scan was frequency dependent. The slope of the laser frequency dependence on the filter rotation angle was thus determined in separate measurements; the data were used by the scanning computer to adjust the stepping rate so that a constant scanning rate of 0.2 $cm^{-1}s^{-1}$ was achieved, independent of laser operating frequency.

The solid etalon consisted of an uncoated, 0.10-cm-thick, quartz plate; the free-spectral range was about 3.44 $cm^{-1}$. The etalon was mounted on a galvanometer; synchronous scanning with the birefringement filter was achieved by driving the galvanometer with a square-root-of-time ramp adjusted to compensate for the $\theta^2$ dependence of the shift of the etalon transmission peaks with $\theta$, the angle between the etalon normal and the laser beam. Varying $\theta$ from slightly greater than 0° to about 4° resulted in linear scans of more than 30 $cm^{-1}$. Walk-off losses at the extreme of the scans were about 20%. Scans were sequenced with a 10.3-$cm^{-1}$ overlap. Backlash in the birefringent filter mechanical drive was automatically compensated for at each resetting of the scan starting frequency; the correction was determined empirically. This correction was essential to achieving long sequences of overlapping scans with no etalon mode hops. Otherwise the peak transmission of the etalon did not coincide with the transmission maximum of the birefringement filter, ultimately leading to etalon mode hops. With this method we have achieved continuous scan lengths of about 600 $cm^{-1}$.

As discussed earlier, when laser 2 was tuned to a LiHe molecular absorption (or to the atomic Li $2p$-$3d$ transition at 610.5 nm) atomic Li fluorescence on the $3p$-$2s$ transition at 323.4 nm resulted. The uv signal was practically background-free and served to monitor the LiHe absorption signal. The fluorescence was collected and focused on the cathode ($S$-20) of a photomultiplier tube (PMT). The PMT was mounted with ultraviolet-transmitting glass filters that effectively eliminated light above 400 nm, including the intense 671.0-nm Li resonance radiation and scattered laser light. The PMT output was sampled at 10 Hz and amplified and processed by a photon counting system; the resulting analog output was displayed on a chart recorder. A portion of the laser 2 output was passed through a 10-cm-long molecular $I_2$ cell heated to about 320 K. The transmitted light was detected by a photodiode. The resulting absorption spectrum was also displayed on the chart recorder. It put the simultaneously recorded LiHe spectrum on an absolute frequency scale within a precision of about 0.20 $cm^{-1}$. A third portion of the laser 2 output was passed through a 0.4987-$cm^{-1}$ etalon; the resulting intensity variations were detected by a photodiode and were displayed on the $y$ axis of an $x$-$y$ recorder. The $x$ coordinate was driven by a linear output from the laser 2 galvanometer drive. The signal served as a monitor of the linearity of the laser 2 scan. Mode hops at the free spectral range of the intracavity etalon (3.44 $cm^{-1}$) were also readily detected.

## III. RESULTS AND ANALYSIS

### A. Overview

We have measured the absorption spectrum of LiHe mixtures in the spectral range 15 900–17 400 $cm^{-1}$. In the absence of laser 1 tuned to the atomic Li resonance transition at 14 903.8 $cm^{-1}$, the spectrum consists solely of atomic absorption at the Na $D1$ and $D2$ lines; the Na is present as an impurity in the Li. When laser 1 was tuned to the Li $2s$-$2p$ transition, the dominant spectral feature was the atomic Li $2p$-$3d$ transition at 16 379.3 $cm^{-1}$; the 0.30-$cm^{-1}$ fine-structure splitting of this transition was clearly resolved. The peak counting rate at this transition was typically $\sim 10^7$ $s^{-1}$. A number ($\sim$30) of considerably weaker absorption features ($10^2$–$10^4$ $s^{-1}$) were also observed in this spectral range; previous experiments[38] have shown these to be molecular LiHe rotation-vibration bands from the $2p\ ^2\Pi$ electronic state to the $3d\ ^2\Delta$, $3d\ ^2\Pi$, $3p\ ^2\Pi$, $3p\ ^2\Sigma^+$ electronic states. Each band consisted of about 10–40 individual transitions in either two or three branches. The bluemost branch of each band showed a distinct band head; they were otherwise red degraded. The first few lines of each branch were generally the narrowest, having a width of about 0.2 $cm^{-1}$ when the He pressure was 50 Torr. The dominant contributors to the observed width are (1) the laser linewidth of about 0.05 $cm^{-1}$, (2) the unresolved molecular LiHe fine structure ($\lesssim$0.2 $cm^{-1}$), and (3) collision and Doppler broadening of the absorption lines. For the lowest He pressures, the dominant width is due to the combined Doppler and fine-structure splitting. With increasing He pressure, the observed width increases rapidly with pressure, for there are many inelastic processes that decrease the effective lifetime of each LiHe rotation-vibration state, e.g., rotational and vibrational energy transfer and collisional dissociation. Data illustrating this effect are presented in Fig. 3 for several $Q$-branch lines of the $^6Li^4He$ $3d\ ^2\Delta(0) \leftarrow 2p\ ^2\Pi(0)$ band. The linewidth is defined as the full width at half maximum of the symmetrical absorption lines. For the $Q(3)$ line the broadening rate is $8(2)\times 10^{-4}$ $cm^{-1}$/Torr, while for the

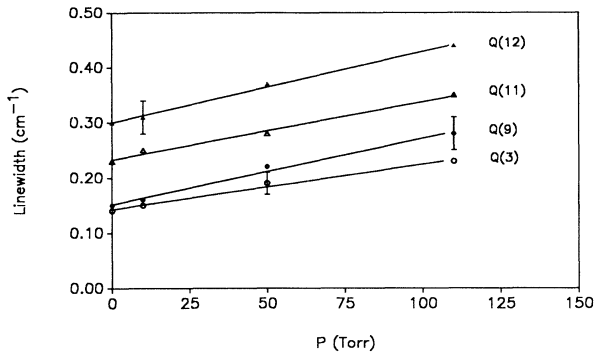


FIG. 3. The observed linewidth of several $Q$-branch lines in the $^6Li^4He$ $3d\,^2\Delta(0)\leftarrow 2p\,^2\Pi(0)$ band as a function of He pressure. The symbols indicating the $P=0$ intercept do not represent data points.

$Q(12)$ line it is $13(3)\times 10^{-4}$ cm$^{-1}$/Torr.

Also evident in Fig. 3 is the increase of the zero-pressure width with increasing $N$. Similar data for the $P(N)$ and $R(N)$ [see $R(11), R(12)$ in Fig. 4] branches show that the increased width is due to dissociation of the upper $3d\,^2\Delta$ $(v=0,N)$ levels. As these levels are energetically well below the $3d\,^2\Delta$ limit, the dissociation is most likely into the continuum of states above the atomic Li $3p$ limit and due to rotational coupling with the $3p\,^2\Pi$ state. Several higher $N$ lines in other $3d\,^2\Delta(v',N')\leftarrow 2p\,^2\Pi(v'',N'')$ transitions also show comparable broadening.

We are concerned in this paper with that portion of the spectrum blue of about 16 650 cm$^{-1}$. In that region we see a distinct progression of six vibrational bands; rotational analysis (next section) has shown these to be due to

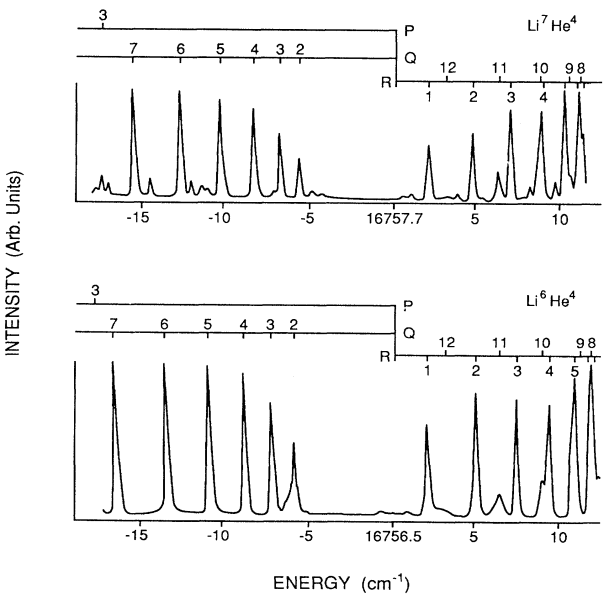


FIG. 4. A comparison of the $3d\,^2\Delta(v'=0)\leftarrow 2p\,^2\Pi(v''=0)$ band origin region for the $^7Li^4He$, $^6Li^4He$ absorption spectra.

the $3d\,^2\Delta\leftarrow 2p\,^2\Pi$ electronic transition in molecular LiHe. Each band has a strong $R$ $(\Delta N=+1)$ and $Q$ $(\Delta N=0)$ branch and a weaker $P$ $(\Delta N=-1)$ branch, consistent with the Hönl–London formulas[42] applicable to this case. The $R$ branch is initially blue degraded, and shows a distinct band head. The $Q$ and $P$ branches are red degraded, and show a peak intensity corresponding to a rotational temperature of about 350 K. Comparison of individual line positions for $^6Li^3He$, $^6Li^4He$, and $^7Li^4He$ show clear isotope shifts in each case. All these features are evident in the band origin region of the $3d\,^2\Delta(0)\leftarrow 2p\,^2\Pi(0)$ transition for $^7Li^4He$ and $^6Li^4He$, shown in Fig. 4. The isotope shifts are readily seen as are relatively weak $^6Li^4He$ impurity lines in the (upper) $^7Li^4He$ spectrum.

### B. Spectral analysis

#### 1. Rotation and vibration

For the LiHe molecular states we have studied, the spin-orbit coupling constants $A(R)$ are small compared to the rotational ones; the angular momentum coupling is expected to be well described by Hund's case (b). This is evident in the measured LiHe spectra; the fine-structure splitting of low-$N$ levels was not observed within the experimental resolution of about 0.2 cm$^{-1}$. This is consistent with eigenenergy expressions[42] for the spin-orbit splitting in a near case (b) $3d\,^2\Delta\leftarrow 2p\,^2\Pi$ transition. However, for larger $N$ we see evidence of weak interactions of the $3d\,^2\Delta$ and $2p\,^2\Pi$ states with other nearby electronic states. Although a qualitative description is given in this paper, we defer a detailed discussion of the interactions (which correspond to couplings $\sim 10^{-3}$ cm$^{-1}$) until analysis of the spectroscopy of the contributing states (see Fig. 1) is complete. We thus consider the spectroscopic constants reported here to be effective ones, having (for the $B$ values) magnetic contributions $\lesssim 10^{-3}$ cm$^{-1}$. In any case, this is much smaller than the statistical uncertainty in the rotational constants for the bands discussed in this paper.

First, for all observed vibrational bands, the largest $N$ lines are seen to broaden, beyond their pressure broadened width, with increasing $N$ (see Figs. 3 and 4). As indicated earlier, these levels are below the dissociation limit for either the $2p\,^2\Pi$ or $3d\,^2\Delta$ state; the most likely origin of the broadening is rotational predissociation of the $3d\,^2\Delta$ state into the $3p\,^2\Pi$ continuum. Second, the higher $N$ lines of the $P$ and $R$ branches in the 0-0 band of each isotope show a just-measurable splitting ($\sim 0.35$ cm$^{-1}$) into two components of about equal intensity. There is no observable doubling of the $Q$-branch lines. The doubling is most readily evident in the $^6Li^3He$ spectrum and is unmeasurable within our resolution for $^7Li^4He$. There is no observable splitting in the other $3d\,^2\Delta(v')\leftarrow 2p\,^2\Pi(v'')$ transitions for any of the isotopic combinations. The observed doubling may be due to a combination of $\Lambda$ doubling in the $2p\,^2\Pi$ and $3d\,^2\Delta$ states. This doubling can add for the $P$ and $R$ branches and subtract for the $Q$ branch. A pure precision estimate[4,42] of the $2p\,^2\Pi$-$2p\,^2\Sigma^+$ interaction gives $q\sim 10^{-3}$ cm$^{-1}$ for

TABLE I. Rotational and rotational distortion constants for the $2p\ ^2\Pi$ and $3d\ ^2\Delta$ vibrational levels. All quantities are in $cm^{-1}$.

| | $^6Li^3He$ | | $^6Li^4He$ | | $^7Li^4He$ | |
|---|---|---|---|---|---|---|
| | $B$ | $D^a$ | $B$ | $D^a$ | $B$ | $D^a$ |
| $^2\Pi(0)$ | 2.470(4) | 0.60(9) | 2.070(6) | 0.25(6) | 1.956(2) | 0.25(4) |
| $^2\Pi(1)$ | 2.123(11) | 0.45(40) | 1.814(8) | 0.37(18) | 1.718(7) | 0.20(16) |
| $^2\Delta(0)$ | 2.236(3) | 0.84(2) | 1.875(3) | 0.57(2) | 1.768(3) | 0.48(2) |
| $^2\Delta(1)$ | 1.807(7) | 1.1(16) | 1.544(8) | 0.61(16) | 1.467(7) | 0.46(16) |
| $^2\Delta(2)$ | 1.363(11) | 2.07(34) | 1.209(7) | 1.03(15) | 1.166(5) | 0.94(9) |
| $^2\Delta(3)$ | 0.888(9) | 2.70(17) | 0.850(6) | 1.49(10) | 0.833(6) | 1.23(9) |
| | $\Pi$ | $\Delta$ | $\Pi$ | $\Delta$ | $\Pi$ | $\Delta$ |
| $B_e$ | 2.644(8) | 2.439(16) | 2.198(7) | 2.032(13) | 2.075(6) | 1.908(12) |
| $\alpha_e$ | 0.347(12) | 0.403(29) | 0.256(9) | 0.313(23) | 0.238(8) | 0.279(21) |
| $\gamma_e$ | | −0.012(8) | | −0.007(6) | | −0.008(6) |
| $D_e{}^a$ | 0.552(144) | 0.533(30) | 0.387(8) | 0.438(21) | 0.422(147) | 0.374(23) |
| $\beta_e{}^a$ | −0.116(285) | 0.615(45) | −0.057(171) | 0.268(22) | −0.253(290) | 0.215(20) |

[a]These values should be multiplied by a factor of $10^{-3}\ cm^{-1}$.

$^6Li^3He$. A preliminary analysis of the $^6Li^3He$ $3p\ ^2\Sigma^+(0)\leftarrow 2p\ ^2\Pi(0)$ band, which extends to $N=23$, gives combination defects consistent with this estimate of $q$. $\Lambda$ doubling is normally considered to be negligible in $^2\Delta$ state;[45] it occurs only via interaction of $^2\Sigma$ states through one or more intermediate $^2\Pi$ states. This conclusion, however, depends on the proximity of the $^2\Pi$ and $^2\Sigma^+$ states to the $^2\Delta$ state. Analysis of the other observed bands in LiHe should clarify the origin of the observed splittings.

Then the rotation-vibration energies may be generally described by[42]

$$T(V,N)=\sum_{i,j} Y_{ij}(V+\tfrac{1}{2})^i[N(N+1)-\Lambda^2]^j\ , \qquad (1)$$

where the $Y_{ij}$ are the usual Dunham coefficients and where $\mathbf{N}=\mathbf{R}+\mathbf{\Lambda}$; $N=\Lambda,\Lambda+1,\ldots$. Our results, however, are expressed in terms of the related, customary mechanical rotational and vibrational constants. The measured term values for each band were fit to the general form

$$\nu=T(V',N')-T(V'',N'') \qquad (2)$$

with $i,j=0$, 1, and 2. The $N$ numbering of each rotational band was assigned according to the usual first- and second-combination differences. The electronic transitions were identified as $^2\Delta\leftarrow{}^2\Pi$ by the presence of three strong branches, the absence of $Q(1)$, $P(1)$, and $P(2)$ lines, and the intensity distribution within each band. Illustrative fits of the second combination differences $\Delta_2$ for the $3d\ ^2\Delta\leftarrow 2p\ ^2\Pi$ 0-0 bands of $^6Li^4He$ and $^7Li^4He$ are shown in Fig. 5. The slope and intercept of each line give $8D_v$ and nearly $4B_v$, where $B_v$ and $D_v$ are the usual rotational and centrifugal distortion constants for a vibrational state $v$. Values of $B_v$ and $D_v$ thus obtained for the $3d\ ^2\Delta$ and $2p\ ^2\Pi$ states are given in Table I.

The band origins were determined by extrapolation of the $Q$ branch, via Eqs. (1) and (2), to the rotationless state. Because $\Lambda\neq 0$ for either state, the band origins are offset from $N=0$ by nearly $B''-4B'$. Band origins, adjusted for the offset, for the six observed transitions are listed in Table II. The band origins of Table II, in combination with the rotational constants of Table I, reproduce nearly all the measured line positions to within about 0.20 $cm^{-1}$, well inside the uncertainty in the individual line positions. Transition energies for each analyzed $3d\ ^2\Delta\leftarrow 2p\ ^2\Pi$ line are given in Table III.

In Fig. 6 the residuals, defined as $\nu-\nu_{\text{fit}}$, are presented as a function of energy for each of the three isotopes. Strongly blended or broadened lines are indicated by open circles. For all other data, given by solid circles, the residuals are well within the combined uncertainty of the measurements and the fit.

The vibrational numbering in the $3d\ ^2\Delta$ state was unambiguously determined from the measured isotope

TABLE II. Band origins for the various observed $3d\ ^2\Delta(v')\leftarrow 2p\ ^2\Pi(v'')$ transitions in $^7Li^4He$, $^6Li^4He$, and $^6Li^3He$.

| Isotope | $V'',V'$ | $\nu_0$ ($cm^{-1}$) |
|---|---|---|
| $^6Li^3He$ | 0,0 | 16 753.1(1) |
| | 0,1 | 16 974.8(2) |
| | 0,2 | 17 116.4(2) |
| | 0,3 | 17 190.9(2) |
| | 1,1 | 16 657.7(3) |
| | 1,2 | 16 799.3(4) |
| $^6Li^4He$ | 0,0 | 16 756.5(1) |
| | 0,1 | 16 966.1(3) |
| | 0,2 | 17 107.5(1) |
| | 0,3 | 17 189.7(2) |
| | 1,1 | 16 669.6(2) |
| | 1,2 | 16 810.9(4) |
| $^7Li^4He$ | 0,0 | 16 757.7(1) |
| | 0,1 | 16 963.2(1) |
| | 0,2 | 17 104.3(1) |
| | 0,3 | 17 188.5(1) |
| | 1,1 | 16 673.3(3) |
| | 1,2 | 16 814.3(2) |

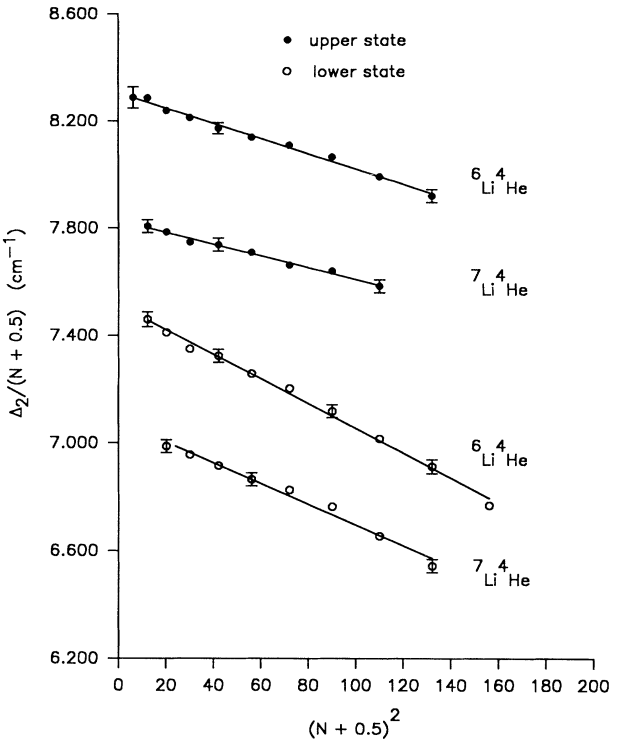


FIG. 5. Second combination differences for the $3d\,^2\Delta(v'=0)\leftarrow 2p\,^2\Pi(v''=0)$ bands of $^7Li^4He$ and $^6Li^4He$. The solid lines represent least-squares fits to the data, and include the effects of rotational distortion.

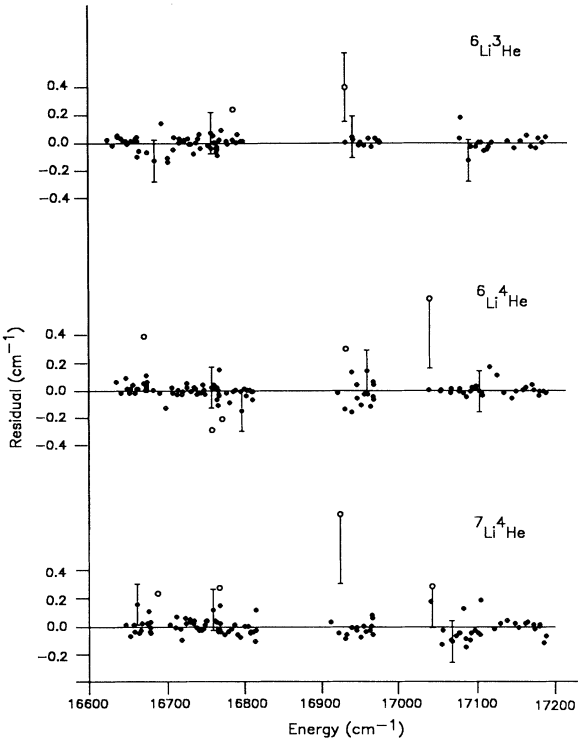


FIG. 6. Residuals of the fits to the measured $3d\,^2\Delta\leftarrow 2p\,^2\Pi$ line positions for $^7Li^4He$, $^6Li^4He$, and $^6Li^3He$.

TABLE III. Measured line positions for the $3d\,^2\Delta(v',N')\leftarrow 2p\,^2\Pi(v'',N'')$ transitions in LiHe. All line positions are in vacuum cm$^{-1}$.

| $N$ | $R(N)$ | $Q(N)$ | $P(N)$ | $N$ | $R(N)$ | $Q(N)$ | $P(N)$ |
|---|---|---|---|---|---|---|---|
| | | $^6Li^3He$ | | 2 | 17 114.8(1) | 17 106.8(1) | |
| (0,0) | | | | 3 | 17 110.6(1) | 17 100.1(1) | |
| 1 | 16 755.1(1) | | | 4 | 17 103.8(1) | 17 090.9(1) | 17 080.7(1) |
| 2 | 16 758.7(1) | 16 745.3(1) | | 5 | 17 094.2(1) | 17 079.5(1) | |
| 3 | 16 761.7(1) | 16 744.0(1) | 16 730.5(1) | (0,3) | | | |
| 4 | 16 764.0(1) | 16 742.1(1) | 16 724.3(1) | 1 | 17 190.3(1) | | |
| 5 | 16 765.7(1) | 16 739.6(1) | 16 717.6(1) | 2 | 17 185.3(1) | 17 180.4(1) | |
| 6 | 16 766.8(1) | 16 736.6(1) | 16 710.4(1) | 3 | 17 177.3(1) | 17 170.7(1) | |
| 7 | 16 767.1(1) | 16 733.0(1) | 16 702.7(1) | 4 | 17 165.5(1) | 17 157.8(1) | |
| 8 | 16 766.6(1) | 16 728.8(1) | 16 694.5(1) | 5 | 17 149.6(1) | 17 141.1(1) | |
| 9 | 16 765.1(1) | 16 723.7(1) | 16 685.6(1) | 6 | | 17 120.4(1) | |
| 10 | 16 762.7(1) | 16 717.8(1) | 16 676.3(1) | (1,1) | | | |
| 11 | 16 759.0(2) | 16 711.1(1) | 16 666.1(1) | 1 | 16 659.2(1) | | |
| 12 | | 16 703.1(2) | 16 655.3(1) | 2 | 16 661.5(1) | 16 650.7(1) | |
| (0,1) | | | | 3 | 16 663.0(1) | 16 648.8(1) | 16 638.1(1) |
| 1 | 16 976.0(1) | | | 4 | 16 663.6(1) | 16 646.1(1) | 16 631.9(1) |
| 2 | 16 976.9(1) | 16 966.1(1) | | 5 | 16 663.6(1) | 16 642.7(1) | 16 625.1(1) |
| 3 | 16 976.4(1) | 16 962.1(1) | 16 951.3(1) | 6 | | 16 638.5(2) | |
| 4 | 16 974.3(1) | 16 956.7(1) | 16 942.5(1) | | | | |
| 5 | 16 970.6(1) | 16 949.8(1) | 16 932.3(1) | (1,2) | | | |
| 6 | | 16 941.5(1) | | 1 | 16 799.8(1) | | |
| 7 | | 16 931.8(2) | | 2 | 16 799.4(1) | 16 791.3(1) | |
| (0,2) | | | | 3 | 16 797.2(1) | 16 786.7(1) | 16 778.6(1) |
| 1 | 17 116.7(1) | | | | | | |

TABLE III. (*Continued*).

| $N$ | $R(N)$ | $Q(N)$ | $P(N)$ | $N$ | $R(N)$ | $Q(N)$ | $P(N)$ |
|---|---|---|---|---|---|---|---|
| 4 | 16 793.1(1) | 16 780.3(1) | 16 769.8(1) | 6 | 16 797.2(1) | 16 781.6(1) | |
| 5 | 16 787.0(1) | 16 772.1(1) | | 7 | | 16 772.3(1) | |
| | | $^6Li^4He$ | | | | $^7Li^4He$ | |
| (0,0) | | | | (0,0) | | | |
| 1 | 16 758.2(1) | | | 1 | 16 759.3(1) | | |
| 2 | 16 761.1(1 | 16 749.8(1) | | 2 | 16 762.0(1) | 16 751.4(1) | |
| 3 | 16 763.6(1) | 16 748.7(1) | 16 737.5(1) | 3 | 16 764.3(1) | 16 750.3(1) | |
| 4 | 16 765.5(1) | 16 747.1(1) | 16 732.1(1) | 4 | 16 766.1(1) | 16 748.7(1) | 16 734.7(1) |
| 5 | 16 766.9(1) | 16 744.9(1) | 16 726.5(1) | 5 | 16 767.6(1) | 16 746.7(1) | 16 729.3(1) |
| 6 | 16 767.9(1) | 16 742.4(1) | 16 720.3(1) | 6 | 16 768.5(1) | 16 744.3(1) | 16 723.5(1) |
| 7 | 16 768.2(2) | 16 739.3(1) | 16 713.8(1) | 7 | 16 768.8(1) | 16 741.4(1) | 16 717.3(1) |
| 8 | 16 768.1(2) | 16 735.8(1) | 16 706.9(1) | 8 | 16 768.7(1) | 16 738.0(1) | 16 710.7(1) |
| 9 | 16 766.9(1) | 16 731.6(1) | 16 699.3(1) | 9 | 16 767.9(1) | 16 734.1(1) | 16 703.6(1) |
| 10 | 16 765.1(1) | 16 726.8(1) | 16 691.5(1) | 10 | 16 766.0(1) | 16 729.6(1) | 16 696.1(1) |
| 11 | 16 762.5(1) | 16 721.3(1) | 16 683.0(1) | 11 | 16 763.6(1) | 16 724.5(1) | 16 688.3(2) |
| 12 | 16 758.7(3) | 16 715.1(1) | 16 674.1(2) | 12 | | 16 718.7(1) | |
| 13 | | 16 708.1(2) | | 13 | | 16 712.2(2) | |
| (0,1) | | | | (0,1) | | | |
| 1 | 16 967.2(1) | | | 1 | 16 964.2(1) | | |
| 2 | 16 968.0(1) | 16 959.0(1) | | 2 | 16 965.1(1) | 16 956.4(1) | |
| 3 | 16 968.0(1) | 16 955.7(1) | 16 946.4(3) | 3 | 16 965.1(1) | 16 953.5(1) | 16 944.6(1) |
| 4 | 16 966.7(1) | 16 951.4(1) | 16 939.4(2) | 4 | 16 964.1(1) | 16 949.6(1) | 16 937.9(1) |
| 5 | 16 964.1(1) | 16 946.2(1) | 16 930.8(1) | 5 | 16 961.7(1) | 16 944.6(1) | 16 930.1(1) |
| 6 | 16 960.3(4) | 16 939.4(2) | 16 921.5(1) | 6 | | 16 938.5(1) | 16 921.4(1) |
| 7 | | 16 931.9(4) | | 7 | | 16 931.6(2) | 16 911.5(1) |
| | | | | 8 | | 16 923.8(2) | |
| (0,2) | | | | (0,2) | | | |
| 1 | 17 107.8(1) | | | 1 | 17 104.6(1) | | |
| 2 | 17 106.7(1) | 17 099.6(1) | | 2 | 17 103.7(1) | | |
| 3 | 17 103.8(1) | 17 094.3(1) | | 3 | 17 101.1(1) | 17 092.0(1) | 17 084.9(1) |
| 4 | 17 099.0(1) | 17 087.3(1) | 17 077.8(1) | 4 | 17 096.8(1) | 17 085.5(1) | 17 076.4(1) |
| 5 | 17 092.1(1) | 17 078.4(1) | 17 066.7(1) | 5 | 17 090.6(1) | 17 077.5(1) | 17 066.0(1) |
| 6 | 17 083.1(1) | 17 067.5(1) | 17 053.8(1) | 6 | 17 082.5(1) | 17 067.4(1) | 17 054.1(1) |
| 7 | | 17 054.5(1) | 17 038.9(1) | 7 | 17 072.7(1) | 17 055.5(1) | 17 040.3(1) |
| 8 | | 17 040.0(1) | | 8 | | 17 042.1(1) | |
| (0,3) | | | | (0,3) | | | |
| 1 | 17 189.3(1) | | | 1 | 17 118.2(1) | | |
| 2 | 17 186.0(1) | 17 181.0(1) | | 2 | 17 185.3(1) | 17 180.4(1) | |
| 3 | 17 180.1(1) | 17 173.7(1) | | 3 | 17 180.1(1) | 17 173.7(1) | |
| 4 | 17 171.6(1) | 17 163.7(1) | | 4 | 17 172.3(1) | 17 164.5(1) | |
| 5 | 17 160.0(1) | 17 150.9(1) | | 5 | 17 161.9(1) | 17 152.9(1) | |
| 6 | 17 145.3(1) | 17 135.3(1) | 17 126.4(1) | 6 | 17 148.7(1) | 17 138.6(1) | 17 129.6(1) |
| 7 | | 17 116.8(1) | | 7 | | 17 121.7(1) | |
| (1,1) | | | | (1,1) | | | |
| 1 | 16 670.9(1) | | | 1 | 16 674.6(1) | | |
| 2 | 16 672.8(1) | 16 663.6(1) | | 2 | 16 676.4(1) | 16 667.7(1) | |
| 3 | 16 674.2(1) | 16 662.0(1) | 16 652.7(1) | 3 | 16 677.8(1) | 16 666.2(1) | 16 657.4(1) |
| 4 | 16 675.0(1) | 16 659.7(1) | 16 647.6(1) | 4 | 16 678.6(2) | 16 664.1(1) | 16 652.7(2) |
| 5 | 16 675.0(1) | 16 657.0(1) | 16 641.8(1) | 5 | 16 678.9(1) | 16 661.6(1) | 16 647.0(1) |
| 6 | 16 674.4(1) | 16 653.6(2) | 16 635.6(1) | 6 | 16 678.6(2) | 16 658.4(2) | |
| 7 | 16 673.1(1) | 16 649.5(1) | | | | | |
| 8 | 16 671.4(2) | | | (1,2) | | | |
| | | | | 1 | 16 814.8(1) | | |
| (1,2) | | | | 2 | 16 814.8(1) | 16 808.0(1) | |
| 1 | 16 811.5(1) | | | 3 | 16 813.8(1) | 16 804.7(1) | |
| 2 | 16 811.5(1) | 16 804.3(1) | | 4 | 16 811.3(1) | 16 800.1(1) | 16 790.9(1) |
| 3 | 16 810.1(1) | 16 800.6(1) | | 5 | 16 807.5(1) | 16 794.3(1) | 16 783.0(1) |
| 4 | 16 807.3(1) | 16 795.7(1) | 16 786.2(1) | 6 | | 16 787.1(1) | 16 773.9(1) |
| 5 | 16 803.1(1) | 16 789.4(1) | 16 777.7(1) | 7 | | 16 778.7(1) | |

TABLE IV. Vibrational constants and dissociation energies for the $2p\ ^2\Pi$ and $3d\ ^2\Delta$ states of LiHe isotopic molecules. All quantities are in $cm^{-1}$.

| | $^6Li^3He$ | | $^6Li^4He$ | | $^7Li^4He$ | |
|---|---|---|---|---|---|---|
| | $\Pi$ | $\Delta$ | $\Pi$ | $\Delta$ | $\Pi$ | $\Delta$ |
| $\omega_e$ | 401.8(1.2) | 314.5(2.1) | 367.4(1.1) | 286.6(2.3) | 356.8(1.1) | 277.5(1.6) |
| $\omega_e x_e$ | 42.3(7) | 49.9(8) | 35.4(6) | 41.0(9) | 33.4(5) | 381.1(6) |
| $\omega_e y_e$ | | 2.2(1) | | 1.5(1) | | 1.3(1) |
| $D_0$ | 833(20) | 459(20) | 845(20) | 468(20) | 847(20) | 469(20) |
| $\mu^{1/2}\omega_e$ | 569.5(1.7) | 445.8(3.0) | 569.6(1.7) | 444.3(3.6) | 569.6(1.8) | 443.0(2.6) |
| $\mu\omega_e x_e$ | 85.0(1.4) | 100.2(1.6) | 85.1(1.4) | 98.5(2.2) | 85.1(1.3) | 97.1(1.5) |
| $\mu^{3/2}\omega_e y_e$ | | 6.3(3) | | 5.6(4) | | 5.3(4) |

shifts of the band origins. Polynomial fits to the vibrational spacings [viz., Eq. (1)] then yielded the mechanical constants for the $3d\ ^2\Delta$ state given in Table IV. Note that these fits require three mechanical constants to fit the three measured vibrational spacings for each isotope. The expansion equation (1) is thus not a compact representation of the data for this strongly anharmonic van der Waal's potential.

In the lower section of Table IV, isotopic mass scaled $3d\ ^2\Delta$ state spectroscopic constants are presented. We see very good agreement with the usual reduced mass dependence of $w_e$ and $w_e x_e$, and agreement at the $2\sigma$ level for $w_e y_e$. It appears that the $w_e y_e$ terms may have an anomalous reduced mass dependence. However, without confirmation of the three-parameter fit for each isotope, with a fourth vibrational spacing, no conclusive statement can be made.

For the $2p\ ^2\Pi$ state, only transitions from two vibrational levels to the $3d\ ^2\Delta$ state have been fully analyzed. Transitions from a third $2p\ ^2\Pi$ vibrational levels to the electronic states in the $3p$ and $3d$ manifolds have been observed. These data (to be presented in a subsequent paper) with the measured isotope shifts of the two observed vibrational levels, yield the $2p\ ^2\Pi$ vibrational numbering given with the band origins in Table II. Values for $w_e$ and $w_e x_e$ for the $2p\ ^2\Pi$ state were determined by assuming that those quantities scaled in the normal way with isotopic mass. A least-squares fit to the three measured vibrational spacings then gave the vibrational constants presented in Table IV. Although values for $w_e y_e$ could, in principle, be obtained by the same method, we found that the precision of the measurements was insufficient to obtain reasonable values for this quantity. Thus the vibrational constants in Table IV should be considered as tentative ones, subject to revision as more experimental data becomes available.

Equilibrium rotational constants were then determined by least-squares fits to the data in Table I (when the data set was large enough) for both the $3d\ ^2\Delta$ and $2p\ ^2\Pi$ electronic states. These numbers are also summarized in Table I.

### 2. *Analysis of results*

The $3d\ ^2\Delta$ state data were further analyzed through an inverted perturbation analysis[46] (IPA). In the IPA method a potential energy curve $V(R)$, which agrees in a least-squares sense with the data, is generated. For the data presented in this paper we have generally represented the potential by the Thakkar[47] form,

$$V(R)=e_0\lambda^2\left[1+\sum_{n=1}^{\infty} e_n\lambda^n\right],$$

where $\lambda=1-(R_e/R)^p$, and where $e_n$ and $p$ are parameters. The equilibrium separation is $R_e$ and the dissociation energy is given by $e_0(1+\sum_n e_n)$.

We have performed extensive IPA numerical studies of the Thakkar potential as applied to the LiHe spectroscopic data; the details of these studies will be presented in another paper.[48] It was generally found, however, that an effective representation of the potential consists of separate choices of $p$ and $\{e_n\}$ for $R<R_e$ and $R>R_e$. For $R<R_e$, only the $e_0$ term was chosen to be nonzero, while for $R>R_e$, all terms ($n\leq 8$) with even $n$ were varied. These choices are flexible enough to represent the data yet eliminate unphysical rollover ($R<R_e$) and oscillations ($R>R_e$) of the potential.

In generating an IPA potential, an initial starting potential is required. To do this, we chose $R_e$ through its relation with $B_e$,[42] and both values of $p'$ and $p$ through their connection[47] with the first Dunham coefficient $a_1$ ($p=a_1-1$). The coefficient $e_0$ was chosen to be larger than the expected dissociation energy, while the other $e_n$ were set initially to 0. For these choices, the $e_n$ and $R_e$ were then varied so as to minimize $\chi^2$ as calculated by

TABLE V. Thakkar potential parameters describing the $^7Li^4He$ IPA $3d\ ^2\Delta$ potential.

| | $R>R_e$ | $R<R_e$ |
|---|---|---|
| $P$ | 5.2 | 4.3 |
| $E(0)$ ($cm^{-1}$) | 616.006 | 359.547 |
| $E(2)$ | −1.263 34 | |
| $E(4)$ | 3.296 85 | |
| $E(6)$ | −3.279 12 | |
| $E(8)$ | 1.242 91 | |
| $R_e$ (units of $a_0$) | 3.572 | |

comparing the original data with the eigenvalues of $V(R)$. Varying $p$ $(R > R_e)$, $p'$ $(R < R_e)$, and $R_e$ from these nominal values maps out a volume in this parameter space where $\chi^2$ is small. Coefficients for an IPA Thakkar potential so generated for the $^7Li^4He$ data are given in Table V; the shape of the potential and the associated vibrational wave functions are displayed in Fig. 7.

We note that the $^7Li^4He$ IPA $3d\ ^2\Delta$ potential presented here yields agreement with the $^7Li^4He$, $^6Li^4He$, and $^6Li^3He$ results to within $\leq 0.1$ cm$^{-1}$, $\leq 0.5$ cm$^{-1}$, and $\leq 1.8$ cm$^{-1}$, respectively, for the individual eigenenergies. For $^6Li^3He$ in particular, this is well outside the accuracy of the data. One possible explanation for this effect is that the $^6Li^3He$ data, due to its smaller reduced mass, extend nearer to dissociation than the $^7Li^4He$ data. A different parametrization of the potential could then yield agreement for all three isotopes. A second possibility is that adiabatic, mass-dependent corrections to the Born-Oppenheimer potential are necessary for the Li-He states studied here. Contamination of the $3d\ ^2\Delta$ rotational constants by the $2p\ ^2\Pi$ $\Lambda$ doubling (discussed in the previous section) is too small to produce a discrepancy of this magnitude. Further analysis is ongoing, and results will be presented in a later paper.[48]

The $3d\ ^2\Delta$ state data presented in this paper do not extend to the dissociation limit. Different choices of the parameters of the IPA Thakkar potential then led to different potentials outside the range of the data. The potentials within the range of the data were nearly indistinguishable. However, there is thus some uncertainty in the binding energy; the spread in the values obtained for different parametrizations of $V(R)$ is about 20 cm$^{-1}$. We take this as a measure of the uncertainty in $D_e$ and in $D_0$, the dissociation energy. A similar spread is found in $R_e$ but in this case is within the uncertainty in $R_e$ as determined from $B_e$.

A long-range vibrational analysis[49] with an assumed long-range potential $-C_6/R^6$ led to an estimate of $D_e = 610(20)$ cm$^{-1}$ for all three isotopes. In the analysis it was assumed that a long-range model is correct, and $D_e$ was varied to fit the data. Note that the result for $D_e$ is not strongly sensitive to the long-range exponent; a choice of $-C_4/R^4$ led to $D_e = 630(20)$ cm$^{-1}$. Finally, we point out that the Thakkar parameter $p$ gives the asymptotic $(R \rightarrow \infty)$ power-law behavior for $V(R)$; our value for $p$ is near the value $(n=4)$ for an $Li^+$-He ion-neutral interaction. In fact, the $3d\ ^2\Delta$ potential is similar in position and depth to the $Li^+He\ ^1\Sigma^+$ ion potential.[50,51] This is consistent with the approximate relative sizes of the Li-He equilibrium separation $(R_e \simeq 3.5a_0)$ and the mean radius[52] of the Li valence electron orbit $(r_e \simeq 10.5a_0)$. As the Li principal quantum number increases, we expect the neutral molecular potentials to go over more closely to the ion potential. Experiments on the spectroscopy of these higher LiHe molecular Rydberg states are in progress. The dissocation energy for the $2p\ ^2\Pi$ state is readily determined from the 0-0 band origin, the $3d\ ^2\Delta$ dissociation energy, and the atomic Li $3d$-$2p$ transition energy. The atomic fine and hyperfine structure is negligible compared to the uncertainty in $D_0$ for the $3d\ ^2\Delta$ state, and so is ignored in the calculation. The binding energy is then readily determined from $D_0$ $(2p\ ^2\Pi)$ and the vibrational parameters listed in Table IV. The equilibrium separation for this state was determined from $B_e$ in the usual manner. Finally, as mentioned previously, we have recently measured absorption from the $v''=2$ vibrational level in the $2p\ ^2\Pi$ state to the $v'=2$ level of the $3d\ ^2\Delta$ state. We defer an IPA analysis of the $2p\ ^2\Pi$ state until analysis of this data is completed. Values for $D_0, D_e, R_e$ for the $2p\ ^2\Pi$ and $3d\ ^2\Delta$ state are summarized in Table VI.

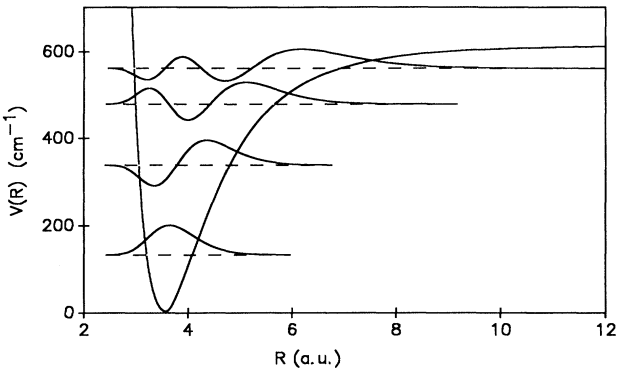


FIG. 7. An IPA potential for the $^7Li^4He\ 3d\ ^2\Delta$ state.

TABLE VI. Comparison of various determinations of the binding energy ($D_e$), and equilibrium separation ($R_e$) for the LiHe $3d\ ^2\Delta$ and $2p\ ^2\Pi$ state.

| | $2p\ ^2\Pi$ | | $3d\ ^2\Delta$ | |
|---|---|---|---|---|
| | $R_e$ (units of $a_0$) | $D_e$ (cm$^{-1}$) | $R_e$ (units of $a_0$) | $D_e$ (cm$^{-1}$) |
| This experiment | 3.37(3) | 1020(20) | 3.52(2) | 610(20) |
| Balling, Wright, and Havey (Ref. 24) | | 850(100) | | |
| Pascale (Ref. 4) | 3.44 | 1025 | 3.74 | 601 |
| Roberts (Ref. 53) | 3.5 | 856 | 3.75 | 554 |
| Jungen and Staemmler (Ref. 15) | 3.42 | 868 | 3.63 | 549 |

| | $2s\Sigma^+$ | |
|---|---|---|
| | $R_e$ (units of $a_0$) | $D_e$ (cm$^{-1}$) |
| Polak-Dingels, Rajan, and Gislason (Ref. 50) | 3.71(7) | 572(46) |
| Gatland *et al.* (Ref. 51) | 3.71 | 596(30) |

## IV. DISCUSSION OF RESULTS

### A. Extent of the data set

The combination of relatively shallow van der Waals potentials and the small reduced mass of the LiHe molecule limits the number of observable rotational transitions within each vibrational band to generally less than 30. Further, the large vibrational constants limit the number of bound vibrational levels to about 5 for the $3d\,^2\Delta$ state and an estimated 6–7 for the $2p\,^2\Pi$ state. Nevertheless, the rotational data for the $3d\,^2\Delta$ state extends to near the dissociation limit, while the highest observed rotational-vibrational level for $^6Li^3He$ ($v'=3, N'=6$) is within about 20 $cm^{-1}$ of dissociation. The spectroscopic data extends over nearly the whole of the $3d\,^2\Delta$ electronic state potential. For the $2p\,^2\Pi$ state, data from the lower 75% of the well was obtained, in addition to the dissociation energy for that state. The high degree of anharmonicity of the adiabatic potentials, however, requires that a relatively large number (compared to the number of observed transitions) of vibrational and rotational constants be used to describe the data.

### B. Comparison of $R_e$ and $D_e$ with other data

In spite of this, qualitative and quantitative conclusions about the nature of binding in the $2p\,^2\Pi$ and $3d\,^2\Delta$ states, and the adiabatic potentials for those states, may be made. Table VI contains a comparison of the results of this work for $D_e$ and $R_e$ with recent theoretical and experimental values for those quantities. We note that well depths and equilibrium radii presented in this paper are considerably different than those reported earlier.[23] The earlier results were based on an assumed Morse potential fit to considerably more limited and less precise spectroscopic data for the $3d\,^2\Delta$ state. The actual data presented here are entirely consistent with that presented in our earlier paper. The results presented in this paper supercede those preliminary results. An overall qualitative agreement for both states is evident and Pascale's $l$-dependent pseudopotential calculations[4] for the $2p\,^2\Pi$ well depth and equilibrium position are in excellent agreement with our experiment. The calculated well depths obtained by Jungen and Staemmler[15] and by Roberts[53] are in less satisfactory agreement, as is the value obtained from the far wing line broadening experiment of Balling, Wright, and Havey.[24] That experimental value of 850(100) $cm^{-1}$ is, however, well within $2\sigma$ of the value obtained in this work 1020(20) $cm^{-1}$. The relatively strong binding in this state is due to penetration of the Li $p$ orbital by the He atom. The absence of $p$ electrons in the He $1s^2$ electron configuration permits the He and $Li^+$ cores to approach each other closely and the normally weak van der Waals interaction to become large. For the $3d\,^2\Delta$ electronic state the calculations all show a shallower well at longer equilibrium separations than the experiment. These quantities are very well determined in the experiments reported here, and refinements in the calculations seem necessary. As discussed previously, our $3d\,^2\Delta$ state results are also in quite good general agreement with the $Li^+He$ ion potential.[50,51] For comparison purposes, several recent determinations of $D_e$ and $R_e$ for the $Li^+He$ $^1\Sigma^+$ potential are also presented in Table VI.

## V. CONCLUSIONS

In summary, we have reported extensive results on the rotationally resolved spectroscopy of the $3d\,^2\Delta \leftarrow 2p\,^2\Pi$ transitions in $^7Li^4He$, $^6Li^4He$, and $^6Li^3He$. These results have been analyzed to obtain equilibrium separations and dissociation and binding energies for the two electronic states. An inverted perturbation approach using a Thakkar potential has yielded an IPA potential for the $^7Li^4He$ $3d\,^2\Delta$ state in excellent agreement with the data. This potential is similar in depth and range to the $Li^+He$ molecular ion ground state. It is expected that the shape of the LiHe $nl\lambda$ potentials for large principal quantum numbers $n$ would approach that of the ion potential in the range of chemical forces. Apparently the $3d\Delta$ orbital, with the small atomic quantum defect[54] $\delta_d=0.002$, is sufficiently diffuse that this limit is being approached even for $n=3$. The binding energy and equilibrium separation for the $2p\,^2\Pi$ state is in excellent agreement with recent calculations by Pascale and consistent with an earlier experimental determination of those quantities.

## ACKNOWLEDGMENTS

The support of this research by the National Science Foundation is greatly appreciated.

[1]E. E. Nikitin, in *The Excited State in Chemical Physics* (Wiley, New York, 1975).
[2]L. Krause, in *The Excited State in Chemical Physics* (Wiley, New York, 1975).
[3]See, for example, C. C. Bouchiat, M. A. Bouchier, and L. C. L. Pottier, Phys. Rev. **181**, 144 (1969).
[4]J. Pascale, Phys. Rev. A **28**, 632 (1983).
[5]M. Phillipe, F. Masnou-Seeuws, and P. J. Valiron, J. Phys. B **12**, L493 (1979).
[6]J. Pascale and J. Vandeplanque, J. Chem. Phys. **60**, 2278 (1974).
[7]E. Czuchaj and J. Sienkiewicz, Z. Naturforsch. Teil A **34**, 694 (1979).
[8]W. E. Baylis, J. Chem. Phys. **51**, 2665 (1969).
[9]F. Masnou-Seeuws, J. Phys. B **15**, 883 (1982).
[10]R. P. Saxon, R. E. Olson, and B. Liu, J. Chem. Phys. **67**, 2692 (1977).
[11]G. Peach, Comments At. Mol. Phys. **11**, 101 (1982).
[12]F. Masnou-Seeuws, M. Philippe, and P. Valiron, Phys. Rev. Lett. **41**, 395 (1978).

[13]R. Düren and G. Moritz, J. Chem. Phys. **73**, 5155 (1980).
[14]E. de Prunelé, Phys. Rev. A **35**, 496 (1987).
[15]M. Jungen and V. Staemmler, J. Phys. B **21**, 463 (1988).
[16]B. C. Laskowski, S. R. Langhoff, and J. R. Stallcop, J. Chem. Phys. **75**, 815 (1981).
[17]M. Dolan and F. Masnou-Seeuws, J. Phys. B **14**, L583 (1981).
[18]M. Krauss, P. Maldonado, and A. C. Wahl, J. Chem. Phys. **54**, 4944 (1971).
[19]R. E. M. Hedges, D. L. Drummond, and A. Gallagher, Phys. Rev. A **6**, 1519 (1972).
[20]D. L. Drummond and A. Gallagher, J. Chem. Phys. **60**, 3426 (1974).
[21]G. York, R. Scheps, and A. Gallagher, J. Chem. Phys. **63**, 1052 (1975).
[22]R. Scheps, Ch. Ottinger, G. York, and A. Gallagher, J. Chem. Phys. **63**, 2581 (1975).
[23]M. D. Havey, S. E. Frolking, and J. J. Wright, Phys. Rev. Lett. **45**, 1783 (1980).
[24]L. C. Balling, J. J. Wright, and M. D. Havey, Phys. Rev. A **26**, 1426 (1982).
[25]M. Ferray, J. P. Visticot, J. Lozingot, and B. Sayer, J. Phys. B **13**, 2571 (1980).
[26]G. M. Carter, D. E. Pritchard, M. Kaplan, and T. W. Ducas, Phys. Rev. Lett. **35**, 1144 (1975).
[27]P. Dehmer and L. Wharton, J. Chem. Phys. **57**, 4821 (1972).
[28]R. Düren, E. Hasselbrink, and G. Moritz, Z. Phys. A **307**, 1 (1982).
[29]R. Düren, W. Gröger, E. Hasselbrink, and R. Liedtke, J. Chem. Phys. **74**, 6806 (1981).
[30]R. Düren and W. Gröger, Chem. Phys. Lett. **56**, 67 (1978).
[31]R. Düren and Liedtke, J. Chem. Phys. **74**, 6995 (1981).
[32]R. Düren, Adv. At. Mol. Phys. **16**, 55 (1980).
[33]R. Ahmad-Bitar, W. P. Lapatovich, D. E. Pritchard, and I. Renhorn, Phys. Rev. Lett. **39**, 1657 (1977).
[34]R. E. Smalley, D. J. Auerbach, P. S. H. Fitch, D. H. Levy, and L. Wharton, J. Chem. Phys. **66**, 3778 (1977).
[35]J. Tellinghuisen, A. Rangone, M. S. Kim, D. J. Auerbach, R. E. Smalley, L. Wharton, and D. H. Levy, J. Chem. Phys. **71**, 1283 (1979).
[36]W. P. Lapatovich, R. Ahmad-Bitar, P. E. Moskowitz, I. Renhorn, R. A. Gottscho, and D. E. Pritchard, J. Chem. Phys. **73**, 5419 (1980).
[37]R. A. Gottscho, R. Ahmad-Bitar, W. P. Lapatovich, I. Renhorn, and D. E. Pritchard, J. Chem. Phys. **75**, 2546 (1981).
[38]M. D. Havey, Phys. Rev. Lett. **48**, 1100 (1982).
[39]G. Aepfelbach, A. Nunnemann, and D. Zimmermann, Chem. Phys. Lett. **96**, 311 (1983).
[40]E. Zanger, V. Schmatloch, and D. Zimmermann, J. Chem. Phys. **88**, 5396 (1988).
[41]J. Hanssen, R. McCarroll, and P. Valiron, J. Phys. B **12**, 899 (1979).
[42]G. Herzberg, *Spectra of Diatomic Molecules,* 2nd ed. (Van Nostrand Reinhold, New York, 1950).
[43]C. Chaleard, B. Dubreuil, and A. Catherinot, Phys. Rev. A **26**, 1431 (1982).
[44]W. J. Wang and M. D. Havey, Phys. Rev. A **29**, 3184 (1984).
[45]R. W. Martin and A. J. Merer, Can. J. Phys. **52**, 1458 (1974).
[46]W. M. Kosman and J. Hinze, J. Mol. Spectrosc. **56**, 93 (1975).
[47]A. J. Thakkar, J. Chem. Phys. **62**, 1693 (1975).
[48]R. P. Meyer, M. D. Havey, and C. J. Lee (unpublished).
[49]R. J. LeRoy and R. B. Bernstein, J. Chem. Phys. **52**, 3869 (1970).
[50]P. Polak-Dingels, M. S. Rajan, and E. A. Gislason, J. Chem. Phys. **77**, 3983 (1982).
[51]I. R. Gatland, W. F. Morrison, H. W. Ellis, M. G. Thackston, E. W. McDaniel, M. H. Alexander, L. A. Viehland, and E. A. Mason, J. Chem. Phys. **66**, 5121 (1977).
[52]H. A. Bethe and E. E. Salpeter, *Quantum Mechanics of One- and Two-Electron Atoms* (Springer, Berlin, 1957).
[53]G. Roberts (private communication). Potentials are calculated using the model potential of G. Peach (Ref. 11).
[54]C. E. Moore, *Atomic Energy Levels,* Natl. Bur. Stand. Ref. Data Ser., Natl. Bur. Stand. (U.S.) Circ. No. 35 (U.S. GPO, Washington, D.C., 1971).